AIAA JOURNAL
Vol. 37, No. 12, December 1999

Coupled Thermo–Piezoelectric–Mechanical Model for Smart Composite Laminates

Aditi Chattopadhyay,* Jingmei Li,† and Haozhong Gu‡
Arizona State University, Tempe, Arizona 85287-6106

A coupled thermo–piezoelectric–mechanical model of composite laminates with surface bonded piezoelectric actuators, subjected to externally applied loads, is developed. The governing differential equations are obtained by applying the principle of free energy and variational techniques. A higher-order displacement field is used to accurately capture the transverse shear effects in laminated composite plates of arbitrary thickness. A double triangular function expansion that satisfies the boundary conditions is used as a solution. Both thermal and mechanical loads are considered, and the effect of actuation is studied. Composite laminates of various thickness and lengths are analyzed. The thermal coupling is shown to have significant effects in both quasi-static and active response analyses.

Nomenclature

a_T	$= c_E/T_0$
b_{ij}	= dielectric permittivity
c_E	= heat capacity
c_{ijkl}	= elastic constants
D_i	= electric displacement vector
d_i	= thermal–piezoelectric coupling constants
E_i	= electric field
e_{ijk}	= piezoelectric constants
k_{ij}	= thermal–mechanical coupling constants
$\boldsymbol{L}_1$	= displacement operator matrix
$\boldsymbol{L}_2$	= piezoelectric operator matrix
$\boldsymbol{l}_1$	= thermal operator vector
$\boldsymbol{N}_1$	= interpolation function matrix for displacements
$\boldsymbol{N}_2$	= interpolation matrices for electric potential variables
$\boldsymbol{N}_3$	= interpolation matrices for thermal variables
q_e	= applied charge density
q_t	= applied heat flux density
S	= entropy
$\dot{S}$	$= \partial S/\partial t$
T	= total thickness of plate
T_0	= initial temperature
t_i	= traction components
u_i	= displacement components at an arbitrary point in plate
u_0, v_0, w_0	= midplane displacements
$\boldsymbol{u}_t$	= global vector of general displacement, piezoelectric and thermal fields
$\boldsymbol{u}_\alpha$	= generalized displacement vector
$\boldsymbol{u}_\theta$	= generalized thermal variable vector
$\boldsymbol{u}_\phi$	= generalized electric potential vector
ε_{ij}	= strain components
θ	= temperature difference between initial and final states
κ_{ij}	= thermal conductivity
σ_{ij}	= stress components
ϕ	= electric potential function
ψ_x, ψ_y	= rotations of a transverse normal at midplane about y and $-x$ axes, respectively

Subscript

$, i$	$= \partial/\partial_{xi}$

Received 22 June 1998; revision received 6 May 1999; accepted for publication 11 May 1999.

*Professor, Department of Mechanical and Aerospace Engineering. Associate Fellow AIAA.
†Graduate Research Assistant, Department of Mechanical and Aerospace Engineering.
‡Postdoctoral Fellow, Department of Mechanical and Aerospace Engineering. Member AIAA.

I. Introduction

THE study of embedded or surface mounted piezoelectric materials in structures has received considerable attention in recent years. The interaction of piezoelectric patches surface bonded to a beam have been studied by Crawley and de Luis.[1] Lee[2] developed a rigorous theoretical formulation for distributed piezoelectric sensors and actuators by applying the classical laminate theory. In his work, the only source of coupling between the electric field and the mechanical displacement field is the linear piezoelectric constitutive equation. Wang and Rogers[3] studied a laminated plate with spatially distributed actuators.

In view of the limitations associated with the classical theory, Tzou and Zhong[4] derived governing equations for piezoelectric shells using the first-order shear deformation theory and included the charge equations of electrostatics. Chandrashekhara and Agarwal[5] developed a finite element model based on the first-order shear deformation theory to address the dynamic behavior of laminated composite plates with integrated piezoelectric sensors and actuators. The formulation is applicable to thin and moderately thick plates. Reddy[6] developed a layerwise theory for plates with surface bonded piezoelectric laminae. Mitchell and Reddy[7] presented a refined hybrid plate theory by combining the layerwise theory and an equivalent single-layer theory (ESL) coupled with linear piezoelectricity to model composite laminates with piezoelectric actuators and sensors. They also addressed the coupling between mechanical deformations and the charge equations of electrostatics.

Because application of many aerospace structures involves operations in extreme hot and cold environments, thermal effect becomes an important issue. The thermal effect was studied by Mindlin[8] and Mukherjee and Sinha.[9] Following their work, the coupled effects of thermopiezoelectricity, based on the classical laminate theory, were addressed by Tauchert.[10] Several finite element approaches were also reported addressing the thermal effect on piezoelectric composite structures by using either classical theory or first-order shear deformation theory.[11–13] Further development was made by Lee and Saravanos,[14,15] who discussed the thermal effect on smart materials based on layerwise laminate theory. However, a known thermal field was assumed in their work.

In this paper, a coupled thermo–piezoelectric–mechanical model is developed for a better understanding of the behavior of smart composite structures with surface bonded piezoelectric materials. The equations of motion are developed using an energy principle. The formulation is based on linear piezoelectricity.[16] A higher-order theory is used for an accurate description of the displacement field.

II. Mathematical Formulation

For the plate shown in Fig. 1, the free energy may be written as follows:

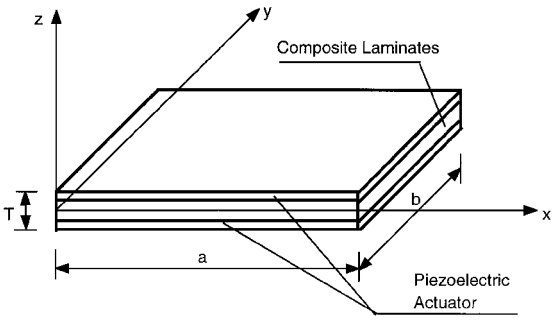

Fig. 1 Geometry of the composite laminates with piezoelectric layers.

$$F(\varepsilon_{ij}, E_i, \theta) = \tfrac{1}{2}c_{ijkl}\varepsilon_{ij}\varepsilon_{kl} - e_{ijk}E_i\varepsilon_{jk} - \tfrac{1}{2}b_{ij}E_iE_j - k_{ij}\theta\varepsilon_{ij} - d_iE_i\theta - \tfrac{1}{2}a_T\theta^2 \quad (1)$$

where the quantities c_{ijkl} and e_{ijk} are the elastic and the piezoelectric constants, respectively, and a_T is defined as c_E/T_0. Consequently,

$$\sigma_{ij} = \frac{\partial F}{\partial \varepsilon_{ij}} = c_{ijkl}\varepsilon_{kl} - e_{ijk}E_k - k_{ij}\theta$$

$$D_i = -\frac{\partial F}{\partial E_i} = e_{ijk}\varepsilon_{jk} + b_{ij}E_j + d_i\theta$$

$$S = -\frac{\partial F}{\partial \theta} = k_{ij}\varepsilon_{ij} + d_iE_i + a_T\theta \quad (2)$$

In vector form, they are

$$\sigma = \boldsymbol{C}\varepsilon - \boldsymbol{PE} - \boldsymbol{k}\theta$$

$$\boldsymbol{D} = \boldsymbol{P}^T\varepsilon + \boldsymbol{BE} + \mathbf{d}\theta$$

$$S = \boldsymbol{k}^T\varepsilon + \boldsymbol{d}^T\boldsymbol{E} + a_T\theta \quad (3)$$

Based on linear piezoelectricity, E_i is derivable from a scalar potential function ϕ as follows:

$$E_i = -\phi_{,i} \qquad (i = 1, 2, 3) \quad (4)$$

The governing equations are now derived using the variational principle, assuming no body force, as follows:

$$0 = -\int_0^{t_0}\int_V \sigma_{ij}\delta\varepsilon_{ij}\,\mathrm{d}V\,\mathrm{d}t + \int_0^{t_0}\int_S t_i\delta u_i\,\mathrm{d}S\,\mathrm{d}t = \delta U + \delta F_1$$

$$0 = -\int_0^{t_0}\int_V D_i\delta\phi_{,i}\mathrm{d}V\,\mathrm{d}t + \int_0^{t_0}\int_S q_e\delta\phi\,\mathrm{d}S\,\mathrm{d}t = \delta E + \delta F_2$$

$$0 = -\int_0^{t_0}\int_V [\kappa_{ij}\theta_{,i}\delta\theta_{,j} + \dot{S}T_0\delta\theta]\,\mathrm{d}V\,\mathrm{d}t + \int_0^{t_0}\int_S q_t\delta\theta\,\mathrm{d}S\,\mathrm{d}t = \delta\Theta_1 + \delta\Theta_2 + \delta F_3 \quad (5)$$

In Eqs. (5), $\dot{S}$ is the derivative of S with respect to time. The quantity V is the laminate volume, and the quantity t is the time span for the dynamic deformation.

Using the third-order shear deformation theory, the displacement field can be written as follows:

$$u_1(x, y, z, t) = u_0(x, y, t) - z\frac{\partial w_0(x, y, t)}{\partial x} + g(z)\psi_x(x, y, t)$$

$$u_2(x, y, z, t) = v_0(x, y, t) - z\frac{\partial w_0(x, y, t)}{\partial y} + g(z)\psi_y(x, y, t)$$

$$u_3(x, y, z, t) = w_0(x, y, t) \quad (6)$$

with

$$g(z) = z - (4/3H^2)z^3 \quad (7)$$

In Eqs. (6), u_i are the displacement components at an arbitrary point in the plate, u_0, v_0, and w_0 are the displacements of a point on the middle plane of the laminate, ψ_x and ψ_y are the rotations of a transverse normal at $z = 0$ about the y and $-x$ axes, respectively, and T indicates the total thickness of the plate (Fig. 1). The expressions for the potential function and the temperature field can be written as follows:

$$\phi^j(x, y, z, t) = \phi_0^j(x, y, t) + z\phi_1^j(x, y, t) \quad (j = 1, 2, 3\ldots) \quad (8)$$

$$\theta(x, y, z, t) = \theta_0(x, y, t) + z\theta_1(x, y, t) \quad (9)$$

By the use of Eqs. (7), the strain vector is written as follows:

$$\varepsilon = \begin{bmatrix}\varepsilon_1\\ \varepsilon_2\\ \varepsilon_4\\ \varepsilon_5\\ \varepsilon_6\end{bmatrix} = \begin{bmatrix}\dfrac{\partial u_1}{\partial x}\\ \dfrac{\partial u_2}{\partial y}\\ \dfrac{\partial u_2}{\partial z} + \dfrac{\partial u_3}{\partial y}\\ \dfrac{\partial u_1}{\partial z} + \dfrac{\partial u_3}{\partial x}\\ \dfrac{\partial u_1}{\partial y} + \dfrac{\partial u_2}{\partial x}\end{bmatrix}$$

$$= \begin{bmatrix}\dfrac{\partial}{\partial x} & 0 & -z\dfrac{\partial^2}{\partial x^2} & g(z)\dfrac{\partial}{\partial x} & 0\\ 0 & \dfrac{\partial}{\partial y} & -z\dfrac{\partial^2}{\partial^2 y} & 0 & g(z)\dfrac{\partial}{\partial y}\\ 0 & 0 & 0 & 0 & \dfrac{\mathrm{d}g(z)}{\mathrm{d}z}\\ 0 & 0 & 0 & \dfrac{\mathrm{d}g(z)}{\mathrm{d}z} & 0\\ \dfrac{\partial}{\partial y} & \dfrac{\partial}{\partial x} & -2z\dfrac{\partial^2}{\partial x\partial y} & g(z)\dfrac{\partial}{\partial y} & g(z)\dfrac{\partial}{\partial x}\end{bmatrix}\begin{bmatrix}u_0\\ v_0\\ w_0\\ \psi_x\\ \psi_y\end{bmatrix} \quad (10)$$

$$= \boldsymbol{L}_1\boldsymbol{u}_u$$

where $\boldsymbol{L}_1$ is an operator matrix and $\boldsymbol{u}_u = [u_0\ \ v_0\ \ w_0\ \ \psi_x\ \ \psi_y]^T$. With

$$\boldsymbol{u}_u = \boldsymbol{N}_1(x, y)\boldsymbol{u}_\alpha \quad (11)$$

where $\boldsymbol{N}_1(x, y)$ is an interpolation matrix for $\boldsymbol{u}_u$, the strain vector now takes the following form:

$$\varepsilon = \boldsymbol{L}_1\boldsymbol{N}_1\boldsymbol{u}_\alpha = \boldsymbol{A}\boldsymbol{u}_\alpha = \boldsymbol{A}'\boldsymbol{u}_t \quad (12)$$

where the general displacement $\boldsymbol{u}_\alpha$ is the first component of the total general displacement field $\boldsymbol{u}_t$ and $\boldsymbol{A}'$ is the enlarged matrix.

The expressions for the electric field $\boldsymbol{E}$ and temperature difference can be derived similarly as follows:

$$\boldsymbol{E}^j = -\begin{bmatrix}\dfrac{\partial\phi^j}{\partial x}\\ \dfrac{\partial\phi^j}{\partial y}\\ \dfrac{\partial\phi^j}{\partial z}\end{bmatrix} = -\begin{bmatrix}\dfrac{\partial}{\partial x} & z\dfrac{\partial}{\partial x}\\ \dfrac{\partial}{\partial y} & z\dfrac{\partial}{\partial y}\\ 0 & 1\end{bmatrix}\begin{bmatrix}\phi_0^j\\ \phi_1^j\end{bmatrix} = -\boldsymbol{L}_2\boldsymbol{u}_\phi^j \quad (j = 1, 2, 3, \ldots) \quad (13)$$

$$\theta = \theta_0 + z\theta_1 = \boldsymbol{I}_1^T\boldsymbol{u}_\theta \quad (14)$$

where $\boldsymbol{u}_\phi^j = [\phi_0^j\ \ \phi_1^j]^T$ is the potential variable vector for the jth layer of piezoelectric laminae. The thermal variable vector is expressed as $\boldsymbol{u}_\theta = [\theta_0\ \ \theta_1]^T$ throughout the thickness of the plate.

The preceding equations can once again be represented using the general displacement field as follows:

$$\boldsymbol{E}^j = -\boldsymbol{L}_2\boldsymbol{N}_2\boldsymbol{u}_\beta^j = -\boldsymbol{M}\boldsymbol{u}_\beta^j = -\boldsymbol{M}'\boldsymbol{u}_t \quad (15)$$

$$\theta = \boldsymbol{I}_1^T\boldsymbol{N}_3\boldsymbol{u}_\gamma = \boldsymbol{p}^T\boldsymbol{u}_\gamma = \boldsymbol{p}'^T\boldsymbol{u}_t \quad (16)$$

where $\boldsymbol{N}_2$ and $\boldsymbol{N}_3$ are the interpolationmatrices for $\boldsymbol{u}_\phi$ and $\boldsymbol{u}_\theta$, respectively The vectors $\boldsymbol{u}_\beta^j$ and $\boldsymbol{u}_\gamma$ are the second and the third components of the total general displacement $\boldsymbol{u}_t$.

The use of Eqs. (3) and Eqs. (10–12) in Eq. (5) and integration with respect to volume V yields the following equations:

$$\delta U = -\int_0^{t_0}\int_V \delta\varepsilon^T\sigma \,\mathrm{d}V\,\mathrm{d}t$$

$$= -\int_0^{t_0}\int_V \delta\boldsymbol{u}_t^T\boldsymbol{A}'^T(\boldsymbol{C}\varepsilon - \boldsymbol{P}\boldsymbol{E} - \boldsymbol{k}\theta)\mathrm{d}V\,\mathrm{d}t$$

$$= -\delta\boldsymbol{u}_t^T\int_0^{t_0}\boldsymbol{K}_1\boldsymbol{u}_t\,\mathrm{d}t$$

$$\delta E = \int_0^{t_0}\int_V \delta\boldsymbol{E}^T\boldsymbol{D}\,\mathrm{d}V\,\mathrm{d}t = -\int_0^{t_0}\int_V \delta\boldsymbol{u}_t^T\boldsymbol{M}'^T(\boldsymbol{P}^T\varepsilon + \boldsymbol{B}\boldsymbol{E} + \mathbf{d}\theta)\,\mathrm{d}V\,\mathrm{d}t = -\delta\boldsymbol{u}_t^T\int_0^{t_0}\boldsymbol{K}_2\boldsymbol{u}_t\,\mathrm{d}t$$

$$\delta\Theta_1 = \int_0^{t_0}\int_V \kappa_{ij}\theta_{,i}\,\delta\theta_{,j}\,\mathrm{d}V\,\mathrm{d}t$$

$$= \int_0^{t_0}\int_V \delta\boldsymbol{q}^T\kappa\boldsymbol{q}\,\mathrm{d}V\,\mathrm{d}t = \delta\boldsymbol{u}_t^T\int_0^{t_0}\boldsymbol{K}_3\boldsymbol{u}_t\,\mathrm{d}t$$

$$\delta\Theta_2 = \int_0^{t_0}\int_V \dot{S}T_0\delta\theta\,\mathrm{d}V\,\mathrm{d}t$$

$$= \int_0^{t_0}\int_V T_0\delta\boldsymbol{u}_t^T\boldsymbol{p}'^T\left(\boldsymbol{k}^T\dot{\varepsilon} + \boldsymbol{d}^T\dot{\boldsymbol{E}} + a_T\dot{\theta}\right)\mathrm{d}V\,\mathrm{d}t$$

$$= \delta\boldsymbol{u}_t^T\int_0^{t_0}\boldsymbol{K}_4\dot{\boldsymbol{u}}_t\,\mathrm{d}t$$

$$\delta F_1 = \int_0^{t_0}\int_S \delta\boldsymbol{u}^T\boldsymbol{t}\,\mathrm{d}S\,\mathrm{d}t = \int_0^{t_0}\int_S \delta\boldsymbol{u}_t^T\boldsymbol{N}_1'^T\boldsymbol{t}\,\mathrm{d}S\,\mathrm{d}t = \delta\boldsymbol{u}_t^T\int_0^{t_0}\boldsymbol{f}_1\,\mathrm{d}t$$

$$\delta F_2 = \int_0^{t_0}\int_S \delta\phi q_e\,\mathrm{d}S\,\mathrm{d}t = \int_0^{t_0}\int_S \delta\boldsymbol{u}_t^T\boldsymbol{N}_2'^T\boldsymbol{l}_1 q_e\,\mathrm{d}S\,\mathrm{d}t$$

$$= \delta\boldsymbol{u}_t^T\int_0^{t_0}\boldsymbol{f}_2\,\mathrm{d}t$$

$$\delta F_3 = \int_0^{t_0}\int_S \delta\theta q_t\,\mathrm{d}S\,\mathrm{d}t = \int_0^{t_0}\int_S \delta\boldsymbol{u}_t^T\boldsymbol{N}_3'^T\boldsymbol{l}_1 q_t\,\mathrm{d}S\,\mathrm{d}t$$

$$= \delta\boldsymbol{u}_t^T\int_0^{t_0}\boldsymbol{f}_3\,\mathrm{d}t \tag{17}$$

where

$$\boldsymbol{q} = \boldsymbol{l}_2\boldsymbol{p}'^T\boldsymbol{u}_t = \boldsymbol{R}'\boldsymbol{u}_t$$

$$\boldsymbol{K}_1 = \int_V (\boldsymbol{A}'^T\boldsymbol{C}\boldsymbol{A}' + \boldsymbol{A}'^T\boldsymbol{P}\boldsymbol{M}' - \boldsymbol{A}'^T\boldsymbol{k}\boldsymbol{p}'^T)\,\mathrm{d}V$$

$$\boldsymbol{K}_2 = \int_V (\boldsymbol{M}'^T\boldsymbol{P}\boldsymbol{A}' - \boldsymbol{M}'^T\boldsymbol{B}\boldsymbol{M}' + \boldsymbol{M}'^T\mathbf{d}\boldsymbol{p}'^T)\,\mathrm{d}V$$

$$\boldsymbol{K}_3 = \int_V \boldsymbol{R}'^T\kappa\boldsymbol{R}'\,\mathrm{d}V$$

$$\boldsymbol{K}_4 = \int_V T_0\left(\boldsymbol{p}'\boldsymbol{k}^T\boldsymbol{A}' - \boldsymbol{p}'\boldsymbol{d}^T\boldsymbol{M}' + \boldsymbol{p}'a_T\boldsymbol{p}'^T\right)\mathrm{d}V$$

$$\boldsymbol{f}_1 = \int_S \boldsymbol{N}_1'^T\boldsymbol{t}\,\mathrm{d}S, \qquad \boldsymbol{f}_2 = \int_S \boldsymbol{N}_2'^T\boldsymbol{l}_1 q_e\,\mathrm{d}S, \qquad \boldsymbol{f}_3 = \int_S \boldsymbol{N}_3'^T\boldsymbol{l}_1 q_t\,\mathrm{d}S \tag{18}$$

By the defining of

$$\boldsymbol{f} = \boldsymbol{f}_1 + \boldsymbol{f}_2 + \boldsymbol{f}_3 \tag{19}$$

the governing equations can be written as follows:

$$\boldsymbol{K}_4\dot{\boldsymbol{u}}_t + (-\boldsymbol{K}_1 - \boldsymbol{K}_2 + \boldsymbol{K}_3)\boldsymbol{u}_t + \boldsymbol{f} = \boldsymbol{0} \tag{20}$$

III. Solution

The displacement vector is assumed to have the following form:

$$\boldsymbol{u} = \begin{bmatrix} u_0 \\ v_0 \\ w_0 \\ \psi_x \\ \psi_y \end{bmatrix} = \begin{bmatrix} \sum_m\sum_n u_{mn}(t)\cos\dfrac{m\pi x}{a}\sin\dfrac{n\pi y}{b} \\ \sum_m\sum_n v_{mn}(t)\sin\dfrac{m\pi x}{a}\cos\dfrac{n\pi y}{b} \\ \sum_m\sum_n w_{mn}(t)\sin\dfrac{m\pi x}{a}\sin\dfrac{n\pi y}{b} \\ \sum_m\sum_n \psi_{x_{mn}}(t)\cos\dfrac{m\pi x}{a}\sin\dfrac{n\pi y}{b} \\ \sum_m\sum_n w_{y_{mn}}(t)\sin\dfrac{m\pi x}{a}\cos\dfrac{n\pi y}{b} \end{bmatrix} \tag{21}$$

whereas the vectors ϕ and $\boldsymbol{\theta}$ take the following form:

$$\phi = \begin{bmatrix} \varphi_0 \\ \varphi_1 \end{bmatrix} = \begin{bmatrix} \sum_m\sum_n \varphi_{mn}^0\sin\dfrac{m\pi x}{a}\sin\dfrac{n\pi y}{b} \\ \sum_m\sum_n \varphi_{mn}^1\sin\dfrac{m\pi x}{a}\sin\dfrac{n\pi y}{b} \end{bmatrix} \tag{22}$$

$$\boldsymbol{\theta} = \begin{bmatrix} \theta_0 \\ \theta_1 \end{bmatrix} = \begin{bmatrix} \sum_m\sum_n \theta_{mn}^0\sin\dfrac{m\pi x}{a}\sin\dfrac{n\pi y}{b} \\ \sum_m\sum_n \theta_{mn}^1\sin\dfrac{m\pi x}{a}\sin\dfrac{n\pi y}{b} \end{bmatrix} \tag{23}$$

By substituting Eqs. (21–23) into Eqs. (10), (13–14), and (17–20), the governing equation can be derived. The components of the total general displacement vector $\boldsymbol{u}_t$ are derived by solving the governing equation. The number of terms, (m, n), used in Eqs. (21–23) is determined by the relative error introduced by truncation. The idea is to select the smallest number of terms while maintaining minimum error. Numerical tests revealed that inclusion of the terms associated with $m, n = 1, 3, 5, 7, 9$ resulted in relative error below 0.1% under the different themal and mechanical load conditions. Therefore, this selection criterion is adopted in the numerical studies.

IV. Results and Discussion

The present theory is validated with a standard finite element code ANSYS. A simply supported unidirectional graphite/epoxy laminate square plate, subjected to thermal load at the top surface of the plate, is used for this purpose. To investigate the transverse shear effect, the dimensions of the plate are selected with fixed length $a = b = 86.36$ mm and variable thickness (Fig. 1). The material properties are listed in Table 1. A finite element model (Fig. 2) using 8-node brick elements with an $8 \times 8 \times 6$ mesh is created using ANSYS to verify the results. The variation of normalized central deflection with the length-to-thickness ratio a/T under thermal loading is presented in Fig. 3 for this case. Coupling effects are ignored in the comparison because ANSYS cannot address this issue. Very good agreement is observed between the results from the higher-order theory and those obtained using ANSYS (Fig. 3). Results are

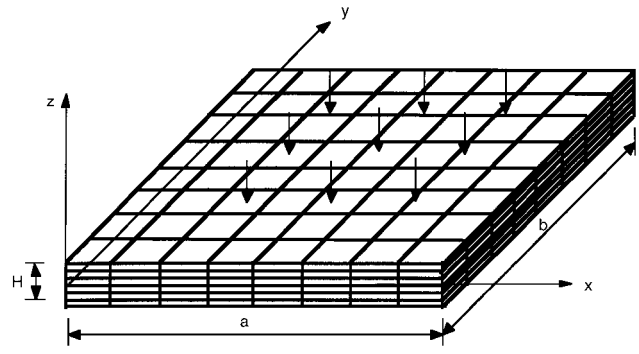

Fig. 2 Finite element mesh ($8 \times 8 \times 6$).

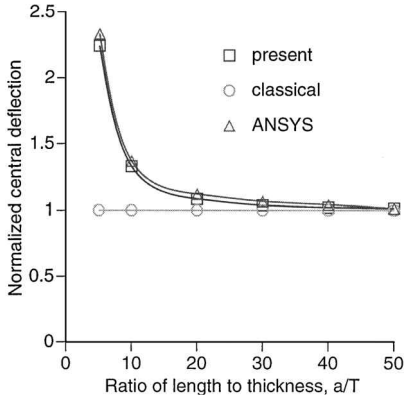

Fig. 3 Model correlation.

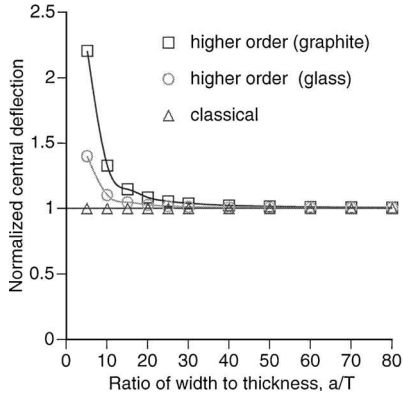

Fig. 4 Comparison of higher-order theory with classical theory, graphite/epoxy, and glass/epoxy.

also compared with those obtained using the classical theory. As shown in Fig. 3, both the classical and higher-order theories predict the same results for thin plates (large a/T value), but significant differences are observed as the plate thickness increases (small a/T values). The higher-order theory is more appropriate for moderately thick or thick plates due to the significant transverse shear effects.

Figure 4 shows the numerical results for both graphite/epoxy and glass/epoxy laminates. The same geometric configuration and load conditions as before are used. Variations of the normalized central deflection with a/T, obtained using the higher-order theory, are compared with those obtained using the classical theory. Solutions for graphite/epoxy laminates show a larger deviation from the classical theory results compared to those obtained using glass/epoxy laminates. Because the tensile to transverse Young's modulus ratio of graphite/epoxy ($E_1/E_2 = 14.95$) is much larger than that of glass/epoxy ($E_1/E_2 = 2.19$), the phenomenon indicates that the transverse shear effects are larger in composites with higher tensile-to-transverse Young's modulus ratio. Because this ratio is generally large for most composite materials, transverse shear effects cannot be ignored.

The thermo–piezoelectric–mechanical coupling effects are investigated for cross-ply graphite/epoxy laminates with a stacking sequence of $[0/90/0]_s$ deg covered by piezoelectric laminae (PZT) on both the top and the bottom surfaces (Fig. 5). The plate is subject to a thermal load on the top and is insulated at the bottom. All four sides are maintained at room temperature (20°C). The dimensions of the plate are such that $a = b = 86.36$ mm, $T = 1.727$ mm, and $h = 1.219$ mm (Fig. 1). A heat flux of 1000 W/m^2 is applied. The engineering constants of the composite material and PZT are listed in Table 1. To understand the effects of the fully coupled formulation, comparisons are made with the results obtained from the following theories: an uncoupled theory and a piezoelectric–mechanical coupled theory with superimposed thermal field. The square data points in Fig. 5 indicate the solution obtained without any coupling effects, the circle data points indicate the solution obtained with piezoelectric–mechanical coupling, and the triangle data points indicate the response with thermo–piezoelectric–mechanical coupling.

Table 1 Material properties of PZT and graphite/epoxy composites

Property	PZT	Graphite/epoxy
Elastic moduli, GPa		
E_{11}	63	144.23
E_{22}	63	9.65
E_{33}	63	9.65
Shear moduli, GPa		
G_{23}	24.6	3.45
G_{13}	24.6	4.14
G_{12}	24.6	4.14
Poisson's ratio		
ν	0.28	0.3
Coefficients of thermal expansion, μm/m · °C		
α_{11}	0.9	1.1
α_{22}	0.9	25.2
Density, kg/m^3		
ρ	7600	1389.23
Piezoelectric charge constant, pm/V		
$e_{31} = e_{32}$	150	——
Electric permittivity, nF/m		
$b_{11} = b_{22}$	15.3	——
b_{33}	15.0	——
Pyroelectric constant, μC/m^2 · °C		
d_3	20	——
Thermal conductivity, W/m · °C		
κ_{11}	2.1	44.8
κ_{22}	2.1	32.1
Heat capacity, J/kg · °C		
c_E	420	1409
Curie temperature, °C		
T_c	365	——

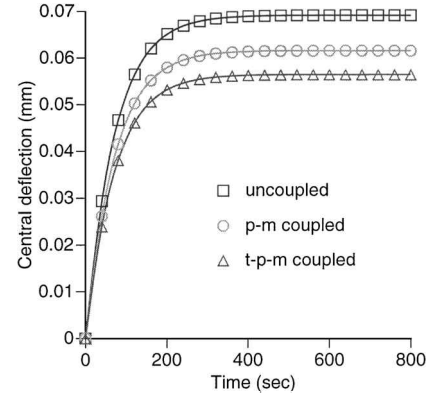

Fig. 5 Coupling effects on quasi-static response.

As seen in Fig. 5, the plate deflection increases gradually with time under thermal load. This is because it takes time for the temperature field to reach the steady state due to thermal conduction from top surface to the remaining surfaces of the plate. In this case, it reaches the steady state in approximately 300 s. With the piezoelectric–mechanical coupling effect, a smaller deflection is observed compared to the case without any coupling effect. A deviation of about 10% is shown in the value of the central deflection. The completely coupled thermo–piezoelectric–mechanical model results in an additional 8% reduction in the value of central deflection. This indicates the presence of a transformation between the thermal, the electrical, and the mechanical energies in the fully coupled case. The reductions are caused by the combined mutual interactions between electrical–mechanical coupling, thermal–electrial coupling, and thermal–mechanical coupling effects. As revealed through detailed analysis, the electrical–mechanical coupling plays a more important role compared to the thermal–mechanical coupling.

A comparison of the uncoupled, the piezoelectric–mechanical coupled and the thermo–piezoelectric–mechanical coupled responses along the width of the same plate under the same loading condition is shown in Fig. 6. Similar trends are once again noted. It must be noted that the maximum deflection occurs at the center due to the simply supported boundary condition. The results indicate

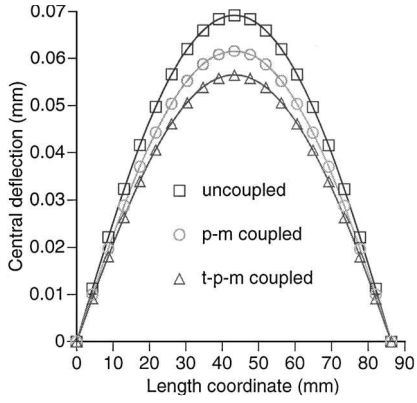

Fig. 6 Variation of central deflections along plate length (square plate).

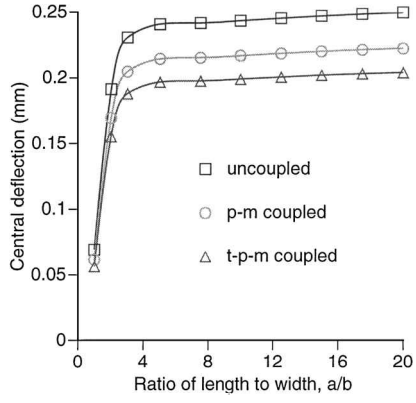

Fig. 7 Variation of central deflection with length-to-width ratio.

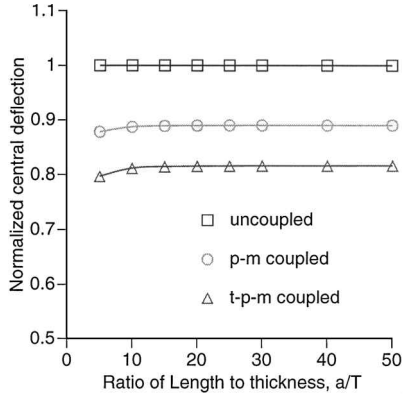

Fig. 8 Variation of central deflection with length-to-thickness ratio.

that the coupling effects play an important role in smart composite applications under thermal load.

The uncoupled and coupled responses are studied by varying the length to width ratio a/b with fixed thickness, $T = 1.727$ mm, and $h = 1.219$ mm (Fig. 7) and the length to thickness ratio $a/b = 1$ for a square plate (Fig. 8). The same material and laminate configurations as before are used in this case. With an increase in the a/b ratio, the deflection initially increases very rapidly (Fig. 7). It is interesting to observe that, in all three cases, the curves flatten as the ratio approaches the value of $a/b = 3$. This is because simply supported boundary condition along the length restricts the plate deformation. Therefore, the plate deflection is bounded, although the plate length increases. For the square plate, normalized central deflection variation with length to thickness ratio a/T, for the uncoupled and the coupled cases, is shown in Fig. 8. With an increase in a/T, the central deflection increases due to the stiffness reduction in the plate. Slightly larger differences between the coupled and the uncoupled cases are observed for thicker plates ($a/T < 10$).

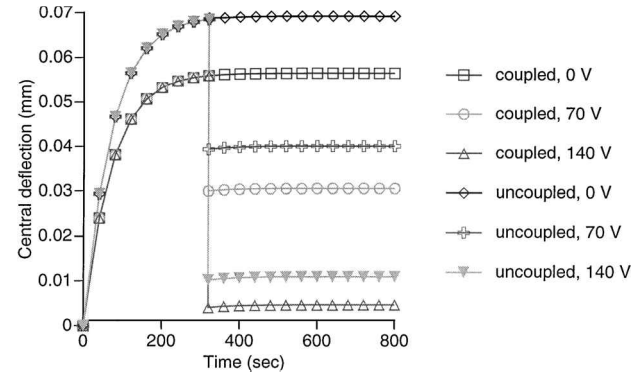

Fig. 9 Coupling effects on quasi-static response with piezoelectric actuation.

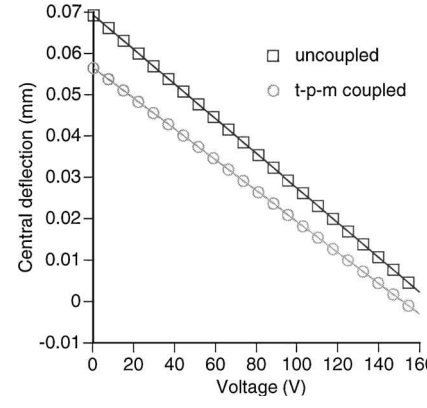

Fig. 10 Variation of central deflection with actuation voltage.

Active deflection control is also studied by applying electrical voltage on the piezoelectric layers to generate mechanical strain. The laminate and piezoelectric configuration and boundary and load conditions are similar to the case shows in Figs. 5 and 6. Deflection reductions due to piezoelectric actuation are shown in Fig. 9 for both uncoupled and completely coupled cases. In both cases, actuation is applied after the plate reaches the steady state. In general, deflections decrease as the applied voltage increases, which is expected. With an applied voltage of 140 V, the central deflection reduces to a near-zero value. This indicates that active control of such structures has the potential to maintain the original shape or to damp out the vibration rapidly. As shown in Fig. 9, a deflection reduction of 0.0519 mm is obtained under actuation in the coupled thermo–piezoelectric–mechanical case, whereas a larger deflection reduction of 0.0583 mm is observed under the same actuation in the uncoupled case. This indicates that the uncoupled theory overpredicts the control authority by 10%.

Actuation, for the same case under different voltages, is shown in Fig. 10. The squared data points indicate the uncoupled central deflection change with variation of actuation voltage. The circled data points indicate the thermo–piezoelectric–mechanical coupled central deflection response under varying voltage. The variations are linear in both cases, but have different slopes. The difference between the coupled and uncoupled cases decreases with increase in voltage. It is once again observed that the deflection reduction under a given voltage is smaller in the coupled case compared to the uncoupled case. This is due to the thermo–piezoelectric–mechanical interaction of energies as noted before. Therefore, once again, ignoring the coupling effects will lead to significant overprediction of control authority.

In summary, the coupling between the thermal, the mechanical, and the piezoelectric effects plays an important role in the response analysis of smart composite structures subjected to thermal loads.

V. Concluding Remarks

A completely coupled thermo–piezoelectric–mechanical approach, based on a higher-order displacement field, has been developed

to study the coupling effects of smart composite plates with piezoelectric actuators and sensors under a thermal load. The principle of free energy and the variational technique are used to obtain the governing differential equations. A refined third-order displacement field is used to capture accurately the transverse shear effects. The resulting theory provides a means for analyzing the completely coupled responses of smart composite structures under thermal loading. The following important observations are made:

1) Current solutions agree very well with those obtained from classical theory for thin plates. However, significant deviations are observed for moderately thick and thick plates. This is due to the presence transverse shear effects, which are neglected by classical theory.

2) Coupling effects significantly decrease plate deflection under thermal load due to the interaction between the thermal, piezoelectric, and mechanical displacement fields.

3) The coupling issues are not affected significantly by plate geometry. Slightly larger differences between the theories are observed for thick plates.

4) The coupled theory provides more accurate evaluation of both thermal and active controls responses. The uncoupled theory overestimates the control authority significantly.

Acknowledgments

The research is supported by the U.S. Air Force Office of Scientific Research, Grant F49620-96-0195; Technical Monitor, Brian Sanders.

References

[1]Crawley, E. F., and de Luis, J., "Use of Piezoelectric Actuators as Elements of Intelligent Structures," *AIAA Journal*, Vol. 31, No. 9, 1987, pp. 1373–1385.

[2]Lee, C. K., "Theory of Laminated Piezoelectric Plates for the Design of Distributed Sensors/Actuators," *Journal of the Acoustical Society of America*, Vol. 87, No. 3, 1990, pp. 1144–1158.

[3]Wang, B.-T., and Rogers, C. A., "Laminate Plate Theory for Spatially Distributed Induced Strain Actuators," *Journal of Composite Materials*, Vol. 25, No. 4, 1991, pp. 433–452.

[4]Tzou, H. S., and Zhong, J. P., "Electromechanics and Vibrations of Piezoelectric Shell Distributed Systems," *Journal of Dynamic Systems, Measurement and Control*, Vol. 115, No. 4, 1993, pp. 506–517.

[5]Chandrashekhara, K., and Agarwal, A. N., "Dynamic Modeling of Piezoelectric Laminated Plates Using Finite Element Method," *Proceedings of Smart Structures and Materials 1993—Smart Structures and Intelligent System*, Vol. 1917, Society of Photo-Optical Instrumentation Engineers, Bellingham, WA, 1993, pp. 451–461.

[6]Reddy, J. N., "A Generalization of Two-Dimensional Theories of Laminated Composite Plates," *Communications in Applied Numerical Methods*, Vol. 3, No. 3, 1987, pp. 173–180.

[7]Mitchell, J. A., and Reddy, J. N., "A Refined Hybrid Plate Theory for Composite Laminates with Piezoelectric Laminae," *International Journal of Solids and Structures*, Vol. 32, No. 16, 1995, pp. 2345–2367.

[8]Mindlin, R. D., "Equations of High Frequency Vibrations of Thermopiezoelectric Crystal Plates," *International Journal of Solids and Structures*, Vol. 10, No. 5, 1974, pp. 625–632.

[9]Mukherjee, N., and Sinha, P. K., "A Finite Element Analysis of Thermostructural Behavior of Composite Plates," *Journal of Reinforced Plastics and Composites*, Vol. 12, No. 10, 1993, pp. 1026–1042.

[10]Tauchert, T. R., "Piezothermoelastic Behavior of a Laminated Plate," *Journal of Thermal Stresses*, Vol. 15, No. 1, 1992, pp. 25–37.

[11]Rao, S. S., and Sunar, M., "Analysis of Distributed Thermopiezoelectric Sensors and Actuators in Advanced Intelligent Structures," *AIAA Journal*, Vol. 31, No. 7, 1993, pp. 1280–1286.

[12]Tzou, H. S., and Howard, R. V., "A Piezothermoelastic Thin Shell Theory Applied to Active Structure," *Journal of Vibration and Acoustics*, Vol. 116, No. 2, 1994, pp. 295–302.

[13]Chandrashekhara, K., and Lolli, M., "Thermally Induced Vibration of Adaptive Doubly Curved Composite Shells with Piezoelectric Devices," *Proceedings of the AIAA/ASME/ASCE/AHS/ASC 36th Structures, Structural Dynamics, and Materials Conference and AIAA/ASME Adaptive Structures Forum*, AIAA, Washington, DC, 1995, pp. 1628–1636.

[14]Lee, H.-J., and Saravanos, D. A., "Active Compensation of Thermally Induced Bending and Twisting in Piezoceramic Composite Plates," *Proceedings of the AIAA/ASME/ASCE/AHS/ASC 37th Structures, Structural Dynamics, and Materials Conference and AIAA/ASME Adaptive Structures Forum*, AIAA, Reston, VA, 1996, pp. 120–130.

[15]Lee, H.-J., and Saravanos, D. A., "The Effect of Temperature Induced Material Property Variations on Piezoelectric Composite Plates," *Proceedings of the AIAA/ASME/ASCE/AHS/ASC 38th Structures, Structural Dynamics, and Materials Conference and AIAA/ASME Adaptive Structures Forum*, AIAA, Reston, VA, 1997, pp. 1781–1788.

[16]Tiersten, H. F., *Linear Piezoelectric Plate Vibrations*, Plenum, New York, 1969, pp. 151–155.

G. M. Faeth
Editor-in-Chief